JOURNAL OF SPACECRAFT AND ROCKETS
Vol. 29, No. 3, May–June 1992

Plasmadynamic Effects in Thermochemical Nonequilibrium Aerobrake Flows

R. A. Mitcheltree* and J. V. Shebalin†
NASA Langley Research Center, Hampton, Virginia 23665

Modifications to the governing equations of thermochemical nonequilibrium hypersonic flow to include plasmadynamic effects are presented. Closure of the resulting equation set requires solution of the magnetic induction equation as an additional field equation. The magnetic field about a 1.1-m nose-radius aerobrake entering the Earth's atmosphere at 80 km altitude and traveling 12 km/s is computed. The result of coupling the additional terms into the Langley Aerothermodynamics Upwind Relaxation Algorithm (LAURA) indicates that plasmadynamic effects are negligible for this two-temperature Mars-return aerobraking simulation. The electromagnetic effects are limited to a small increase in vibrational-electronic temperature in the shock precursor region that does not translate to any change in the properties within the shock layer. A two-temperature solution for a lunar return aerobraking case likewise does not predict any important effects on the flowfield. Arguments are also presented to support the same conclusions for three-temperature solutions.

Nomenclature

B = magnetic field
c_s = mass fraction of species s
D_s = effective diffusion coefficient for species s, m^2/s
$\hat{D}_s$ = average vibrational energy of molecules created, J/kg
E = electric field, T-m/s
E_t = total energy per unit mass, J/kg
e = electron charge
e_e = electron-electronic energy, J/kg
e_v = mixture vibrational energy, J/kg
$e_{v,s}$ = vibrational energy of species s, J/kg
$e^*_{v,s}$ = vibrational energy of species s at T, J/kg
$e^{**}_{v,s}$ = vibrational energy of species s at T_e, J/kg
H = total enthalpy per unit mass, J/kg
h_s = enthalpy per unit mass of species s, J/kg
$h_{e,s}$ = electronic enthalpy per unit mass of species s, J/kg
$h_{v,s}$ = vibrational enthalpy of species s, J/kg
$\hat{I}_s$ = first ionization energy of species s, J/kg-mole
j = electric current, A/m^2
k = Boltzman constant, 1.3807×10^{-23} J/K
M_s = molecular weight of species s, kg/kg-mole
n_i = number density of ions, m^{-3}
n_e = number density of electrons, m^{-3}
$\dot{n}_{e,s}$ = rate of production of species s by electron impact ionization, kg-mole/m^3-s
p = pressure, Pa
P_e = electron pressure, Pa
$\bar{R}$ = universal gas constant, 8314.4 J/kg-mole-K
T = translation-rotational temperature, K
T_e = electron-electronic excitation temperature, K
T_V = vibrational-electron-electronic temperature, K
T_v = vibrational temperature, K
T^* = electronic excitation temperature, K
t = independent variable for time, s
u_j, u = velocity vector, m/s
$\dot{w}_s$ = mass rate of production of species s, kg/m^3-s
x^j = position vector in three dimensional space, m
$\gamma_{e,s}$ = effective collision frequency, s^{-1}
η = thermal conductivity, J/m-s
η_e = thermal conductivity for electronic energy, J/m-s
η_v = thermal conductivity for vibrational energy, J/m-s
μ_0 = magnetic permeability, H/m
ρ = mixture density, kg/m^3
ρ_s = species mass density, kg/m^3
σ = plasma electrical conductivity, A/V-m
$\tau_{i,j}$ = stress tensor, Pa
τ_e = electronic to vibrational energy relaxation time, s
$\langle \tau_{es} \rangle$ = electronic-vibrational energy relaxation time for species s, s
$\langle \tau_s \rangle$ = translational-vibrational relaxation time, s

Introduction

AEROBRAKING, as a means of efficiently decelerating space vehicles into the Earth's atmosphere, is currently being considered for numerous NASA missions. Studies[1-3] have shown that atmospheric entry at the speeds expected for some of these missions produces nonequilibrium flowfields characterized by rapid dissociation and up to 25% ionization of the ambient gas. The flow of this ionized gas, or *plasma,* may include significant plasmadynamic effects that are usually neglected in aerothermodynamic analyses.

Shebalin[4] approximated the magnitude of these effects using a simplified model of the plasma flowfield. His results indicate that the steep gradients in electron number density and temperature across the shock transition layer are a source of potentially large magnetic fields, electric currents, and ohmic heating. Shebalin's work identified the thermoelectric term in the magnetic induction equation, a term that is neglected in standard magnetohydrodynamic (MHD) analysis, as the major source of these effects. His conclusions, however, are limited by the approximations incorporated in his simplified model.

Recently, Palmer[5] performed a detailed computation of the electromagnetic field about a Mars return aerobrake entering at 13.2 km/s, 64.8 km altitude. He concluded that the induced plasmadynamic phenomena had little effect on the fluid flow. He also demonstated that large applied magnetic fields can

Received Dec. 14, 1991; presented as Paper 92-0573 at the AIAA 30th Aerospace Sciences Meeting, Reno, NV, Jan. 6-9, 1992; revision received Feb. 4, 1992; accepted for publication Feb. 5, 1992.

*Aerospace Engineer, Aerothermodynamics Branch, Space Systems Division. Member AIAA.

†Aerospace Technologist, Antenna and Microwave Research Branch, Guidance and Control Division. Member AIAA.

alter the flowfield around an aerobrake. Although his approach accounted for chemical nonequilibrium effects, it did not include thermal nonequilibrium effects.

Plasmadynamic effects result from the presence of induced electric and magnetic (electromagnetic) fields. These fields exist when electric currents form as a result of the motion of charged particles. Electromagnetic fields of sufficient strength to affect the fluid flow might exist in the high gradient, ionizing region of the strong bow shock of an aerobrake. Calculating these fields requires accurate description of the distribution of electronic energy. The assumption of thermal equilibrium assumes the distribution of energy in the electronic and electron-translational modes forms a Boltzman distribution at the single, heavy-particle temperature. This assumption is considered acceptable if the thermal nonequilibrium effects are restricted to a very small region around the shock. It is in this region, however, that electric currents may form. The assumption of thermal equilibrium, therefore, may not provide sufficient detail to accurately predict the induced electromagnetic fields. Furthermore, the feedback mechanism by which plasmadynamics affect the flowfield is an increase in electron translational energy that is then redistributed to the other energy modes in the flowfield: a thermal nonequilibrium process. Thermal equilibrium assumes this redistribution occurs instantaneously and may mask some significant, transient processes.

A large range of peak-heating altitude and velocity combinations are possible for re-entry into the Earth's atmosphere upon return from Mars. The accompanying flowfields have been shown[1] to range from those dominated by both thermal and chemical equilibrium to those dominated by thermochemical nonequilibrium. Although the conditions selected by Palmer[5] represent a chemical nonequilibrium but thermal equilibrium flowfield (justifying his use of a one-temperature solution), the present work will examine a condition dominated by both chemical and thermal nonequilibrium.

The present work performs a detailed computation of the induced electromagnetic fields at aerobraking re-entry conditions characteristic of return from Mars and the Moon into the Earth's nitrogen-rich atmosphere. Thermal nonequilibrium and chemical nonequilibrium effects are included. The objective is to estimate the importance of plasmadynamic effects for aerobrake-re-entry flows in the Earth's atmosphere. The results using a two-temperature flowfield calculation indicate that plasmadynamic effects are negligible for these aerobraking conditions. Arguments are also presented to support the same conclusion for a three-temperature model.

Governing Equations

In Ref. 6, Lee presents the governing equations for the low-density, high-enthalpy flow expected around aeroassisted orbital transfer vehicles. The equations are expressions for the conservation of mass, momentum, and energy. Conservation of mass requires a species conservation equation for each of

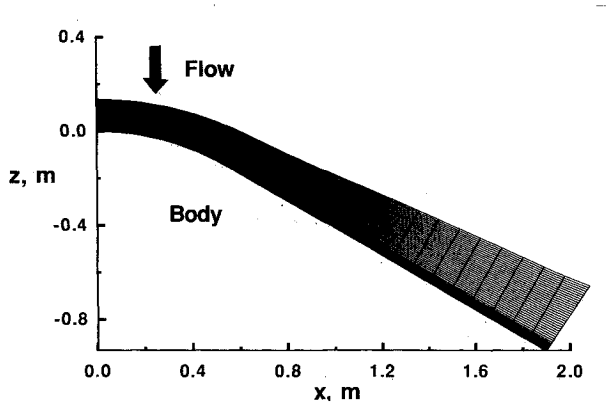

Fig. 1 Axisymmetric aerobrake geometry and 24×64 computational grid.

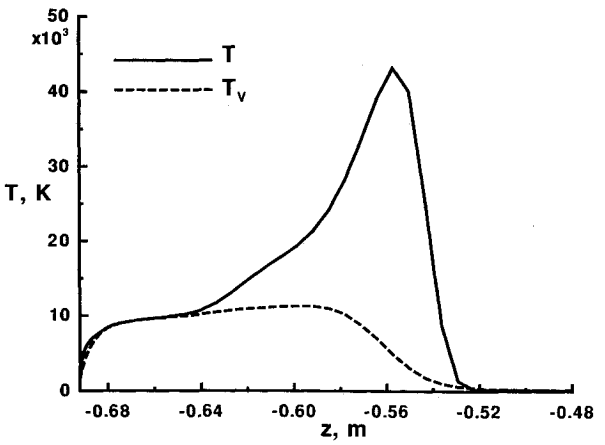

Fig. 2 Temperature profiles across the shock layer on the body flank ($x = 1.5$) for the Mars-return test case.

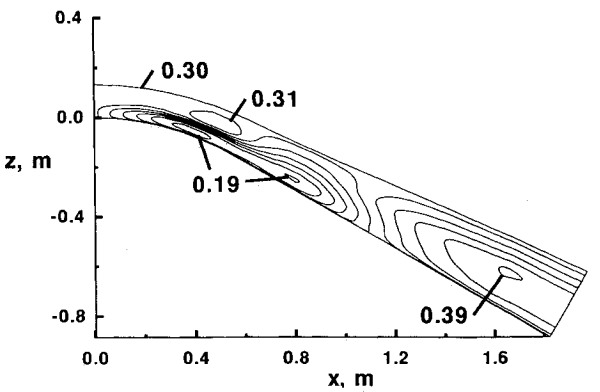

Fig. 3 Contours of the uncoupled magnetic field strnegth on the 24×64 grid (G).

the 11 species, N_2, O_2, N, O, NO, ions of each, and free electrons:

$$\frac{\partial \rho_s}{\partial t} + \frac{\partial}{\partial x^j}\rho_s u^j = \frac{\partial}{\partial x^j}\left(\rho D_s \frac{\partial c_s}{\partial x^j}\right) + \dot{w}_s \tag{1}$$

Diffusion velocities in Eq. (1) are specified via the relations of Hirschfelder et al.[7] using the assumption of ambipolar diffusion to specify the effective diffusion coefficients for the ions and the electrons. Although these effective coefficients are not precise for flowfields with nonzero electric currents, their use should not alter the qualitative conclusions drawn.

For conservation of momentum, the gas mixture can be treated as a three component plasma. This necessitates separate momentum equations for the electrons, ions, and neutrals. Most computational tools for calculating re-entry flows assume no electric currents in the flowfield. Under this zero-current assumption, the electron and ion momentum equations are combined to form an approximate expression for the electric field:

$$E = -\frac{1}{n_e e}\nabla P_e \tag{2}$$

Only an overall momentum equation is then solved.

To allow nonzero currents while still assuming no substantial charge separation (i.e., $n_i \approx n_e$), Eq. (2) becomes:

$$E + u \times B = \frac{j}{\sigma} + \frac{1}{en_e}(j \times B - \nabla P_e) \tag{3}$$

which introduces the magnetic field into the equation set. The present study will use this expression for the electric field. This equation, still an approximate form of the combined electron

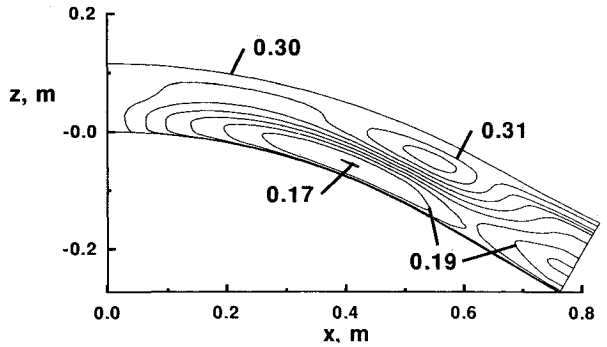

Fig. 4 Contours of the magnetic field strength on the 30 × 128, high-resolution, nose-region grid (G).

and ion momentum equations, is also called the generalized Ohm's law. The overall momentum equation solved is now

$$\frac{\partial}{\partial t}\left(\rho u^i\right) + \frac{\partial}{\partial x^j}\left(\rho u^i u^j\right) + \frac{\partial p}{\partial x^i} - \frac{\partial \tau_{i,j}}{\partial x^j} = (j \times B)^i \tag{4}$$

where the magnetic force term on the right-hand side of the equation is the only addition to this equation when Eq. (3) is used to describe the electric field instead of Eq. (2).

Accurate description of the distribution of particles across the various energy modes in a three-component plasma requires a three-temperature model. A three-temperature model includes conservation equations for the electron-electronic energy, the vibrational energy, and the total energy. Using Eq. (3), the conservation of electron-electronic energy is

$$\frac{\partial}{\partial t}\rho e_e + \frac{\partial}{\partial x^j}\left[u^j(\rho e_e + P_e)\right] = u^j \frac{\partial P_e}{\partial x^j} + \frac{\partial}{\partial x^j}\left(\eta_e \frac{\partial T_e}{\partial x^j}\right)$$

$$+ \frac{\partial}{\partial x^j}\left(\rho \sum_{s=1}^{11} h_{e,s} D_s \frac{\partial c_s}{\partial x^j}\right) + 2\rho_e \frac{3}{2}\bar{R}(T - T_e)\sum_{s=1}^{10}\frac{\nu_{es}}{M_s}$$

$$- \sum_{s=6}^{10} \dot{n}_{e,s}\hat{I}_s - \sum_{s=\text{mol.}} \rho_s \frac{(e_{v,s}^{**} - e_{v,s})}{\langle \tau_{es} \rangle} + (j \cdot E)$$

The conservation of vibrational energy is

$$\frac{\partial}{\partial t}\rho e_v + \frac{\partial}{\partial x^j}\rho e_v u^j = \frac{\partial}{\partial x^j}\left(\eta_v \frac{\partial T_v}{\partial x^j}\right)$$

$$+ \frac{\partial}{\partial x^j}\left(\rho \sum_{s=1}^{11} h_{v,s} D_s \frac{\partial c_s}{\partial x^j}\right) + \sum_{s=\text{mol.}} \rho_s \frac{(e_{v,s}^{*} - e_{v,s})}{\langle \tau_s \rangle}$$

$$+ \sum_{s=\text{mol.}} \rho_s \frac{(e_{v,s}^{**} - e_{v,s})}{\langle \tau_{es} \rangle} + \sum_{s=\text{mol.}} \dot{w}_s \hat{D}_s$$

and the total energy equation becomes

$$\frac{\partial}{\partial t}\rho E_t + \frac{\partial}{\partial x^j}\rho H u^j = \frac{\partial}{\partial x^j}\left(\eta \frac{\partial T}{\partial x^j} + \eta_v \frac{\partial T_v}{\partial x^j} + \eta_e \frac{\partial T_e}{\partial x^j}\right)$$

$$+ \frac{\partial}{\partial x^j}\left(\rho \sum_{s=1}^{11} h_s D_s \frac{\partial c_s}{\partial x^j}\right) + \frac{\partial}{\partial x^j} u^i \tau_{i,j} + (j \cdot E)$$

The total specific energy is now

$$E_t' = \frac{u_i u_i}{2} + \sum_{s=1}^{11} \frac{\rho_s e_s}{\rho} + \frac{B_i B_i}{2\mu_0 \rho} \tag{5}$$

Allowing nonzero currents, i.e., using Eq. (3) for the electric field, results in an additional term in the electron-electronic energy equation and the total energy equation. This term, $j \cdot E$, is called the ohmic heating. When Eq. (2) is used to describe the electric field (zero-current assumption), the work done on the electrons by the electric field is represented in the electron-electronic energy equation by

$$u^j \frac{\partial P_e}{\partial x^j} \tag{6}$$

Using Eq. (3), this term becomes

$$u^j \frac{\partial P_e}{\partial x^j} + (j \cdot E) \tag{7}$$

Ohmic heating is the frictional heating of free electrons caused by differences in the electron velocity and heavy particle velocities. This heating is analogous to the heating that occurs in a current-conducting electrical wire.

In addition to empirical correlations for the chemical reaction rates, thermodynamics, transport properties, and relaxation processes, the previous equation set now requires additional information about the magnetic field to affect closure. These additional empirical relations, Maxwell's equations, are

$$\frac{\partial B}{\partial t} = -\nabla \times E \tag{8}$$

$$j = \frac{1}{\mu_0}\nabla \times B \tag{9}$$

$$\nabla \cdot j = 0 \tag{10}$$

$$\nabla \cdot B = 0 \tag{11}$$

Combining Eq. (8) with Eq. (3) yields the magnetic induction equation:

$$\frac{\partial B}{\partial t} = \nabla\left[u \times B - \frac{j}{\sigma} + \frac{1}{en_e}\nabla P_e - \frac{1}{en_e}(j \times B)\right]$$

Using the perfect gas law and some vector identities this equation becomes

$$\frac{\partial B}{\partial t} = \nabla \times \left[u \times B - \frac{j}{\sigma} - \frac{1}{en_e}(j \times B)\right] + \frac{k}{e}\nabla T_e \times \nabla \ell n\, n_e \tag{12}$$

The last term in the magnetic induction equation is the thermoelectric term. The $j \times B$ term is the Hall term. Both of these terms are usually neglected in the study of magnetohydrodynamics. For the present, they are retained. Equation (9) serves as the definition of current. Equations (10) and (11) will be satisfied identically for the assumption of axisymmetric flow in the test cases of this study.

The modifications to the governing equations to allow nonzero currents for a three temperature model include addi-

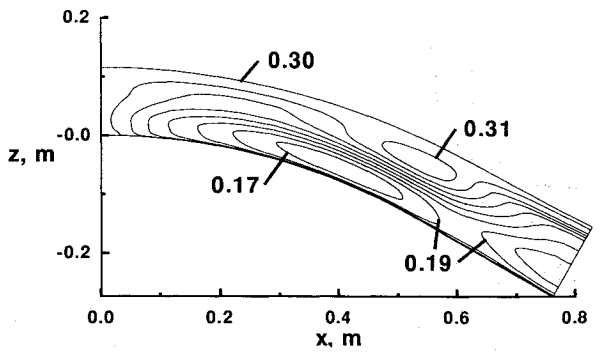

Fig. 5 Contours of the magnetic field strength on the 30 × 128, high-resolution, nose-region grid using fourth-order accurate spatial differencing (G).

tional terms added to the overall momentum equation, the electron-electronic energy equation, and the total energy equation. The magnetic induction equation, Eq. (12), is then solved to calculate these added terms.

Flowfield Solution

In the present study, the Langley Aerothermodynamic Upwind Relaxation Algorithm (LAURA) of Gnoffo et al.[8] is used to provide the flowfield solution. LAURA is a robust tool for analyzing hypersonic flows in thermal and chemical nonequilibrium. The partitioning of energy in LAURA is modeled by Park's two-temperature approximation.[9] Temperature T describes the translational and rotational modes (rotational for molecular species) of all species, and T_V describes the vibrational, electronic, and electron-translational modes. For the latter, this assumes the vibrational and electronic state of all heavy particles and the translational energy state of the free electrons are in equilibrium and described by a Maxwell-Boltzman distribution at temperature T_V. If T_v is the vibrational temperature, T^* is the electronic temperature for the bound electrons, and T_e is the electron translational temperature, the two-temperature assumption sets

$$T_V = T_v = T^* = T_e \tag{13}$$

Therefore, the two-temperature model is a contraction of the three-temperature model. The electron-electronic energy equation is combined with the vibrational energy equation to form a single vibrational-electron-electronic energy equation. The total energy equation remains unchanged.

The two-temperature assumption that justifies the combination of the vibrational, electronic, and electron-translational energy modes into one energy pool assumes the transfer of energy among these modes is instantaneous, i.e., they are always in equilibrium. In reality, this energy transfer is a finite rate process. If the time scale of this energy transfer is not faster than the time scale of the flow for these re-entry conditions, the free electrons just outside the shock, where n_e is only about 10^3 cm^{-3}, will realize a significant increase in energy per electron due to the ohmic heating. The electron temperature would be larger than the vibrational temperature if this occurs and the two-temperature assumption would not be allowable. A three-temperature model, which solves the three separate energy equations, would be required. These more complex models, however, are not widely used because of uncertainties in the relaxation rate $\langle \tau_{e,s} \rangle$ of electron-electronic energy into the vibrational mode.

Hansen[10] has estimated the time scale of the relaxation of electron-electronic energy into vibrational energy for air to be

$$n\tau_e \approx 10^{-18} \frac{\text{s}\cdot\text{mole}}{\text{cm}^3} \tag{14}$$

which is three orders of magnitude faster than the vibrational to translational relaxation times. The transfer of electron-translational energy to the bound electronic mode is theorized[10] to be even faster, which is why the three-temperature model combines these two modes into the electron-electronic energy mode. In the precursor region of the Mars return case, Hansen's time scale of Eq. (14) predicts a relaxation time of 10^{-9} s. The electrons will give up their newly acquired energy before their averaged motion carries them 0.012 mm towards the body. If this estimate is correct, the transfer of energy will be instantaneous for the scale of the test case and the two-temperature model assumption is correct.

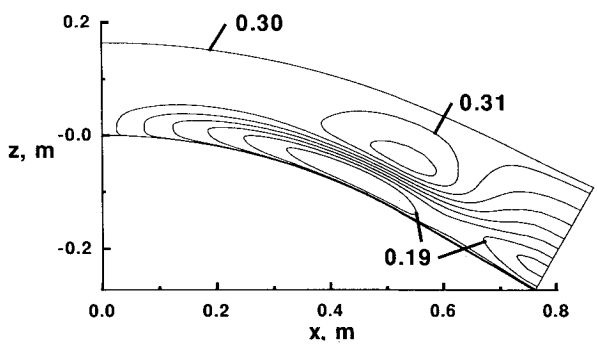

Fig. 6 Contours of the magnetic field strength on the 30×128, increased-grid-extent grid (G).

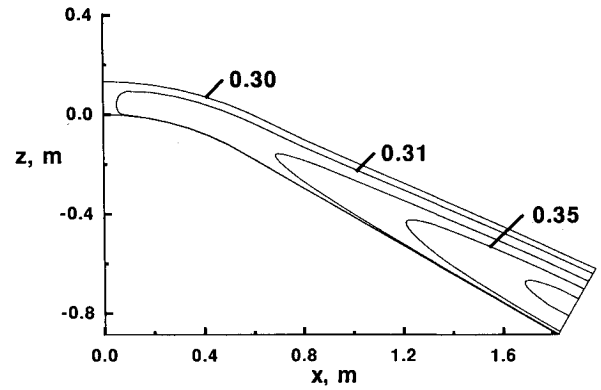

Fig. 7 Contours of the magnetic field strength on the 24×64 grid without the thermoelectric term (G).

For the results presented, constant temperature (1500 K), fully catalytic wall boundary conditions are used. Chemical reaction rates are from Park et al.[11] and the thermodynamic and transport properties of Gupta et al.[12] are used. The numerical formulation of the LAURA algorithm is presented in Ref. 13. A description of the numerous physical models in LAURA appears in Ref. 8.

Coupling plasmadynamic effects into the flowfield calculation requires solution of the magnetic induction equation alongside the gasdynamic equations with the added terms included as described earlier. The important coupling term is the ohmic heating in Eq. (7) that is added to the electron-electronic energy equation. Since LAURA is only a two-temperature model, the term in Eq. (7) is added to the combined vibrational-electron-electronic equation for T_V.

Magnetic Field Solution

The magnetic induction equation, Eq. (12), is three equations for the three components of $\boldsymbol{B}$. The test cases examined in this study are axisymmetric about the z axis and solved in the $y = 0$ plane. The x and z components of $\boldsymbol{B}$ are decoupled from the dominant y component. In fact, these lesser components of $\boldsymbol{B}$ will be small and are neglected—their contribution will depend on the orientation of the vehicle to the Earth's magnetic field. Thus, the assumption is

$$\boldsymbol{B} = B\hat{y} \tag{15}$$

where $\hat{y}$ is a unit vector in the y coordinate direction.

A finite difference method is used to solve the magnetic induction equation separate from the LAURA algorithm. A steady-state form of the equation is written in second-order accurate, finite difference form using grid metrics to form derivatives. An algebraic relation for the value of B at a cell center based on its neighbor's values and the local flowfield solution establishes a fixed point, two-level iteration that converges rapidly. Time asymptotic approaches to solving the magnetic induction equation were also examined but found to be very inefficient because of the inherent stiffness in the equation.

The boundary condition at the freestream boundary sets B equal to a constant value of 0.3 G that is representative of the Earth's magnetic field at the altitudes considered. No current is allowed across the line of symmetry, $x = 0$, or the body

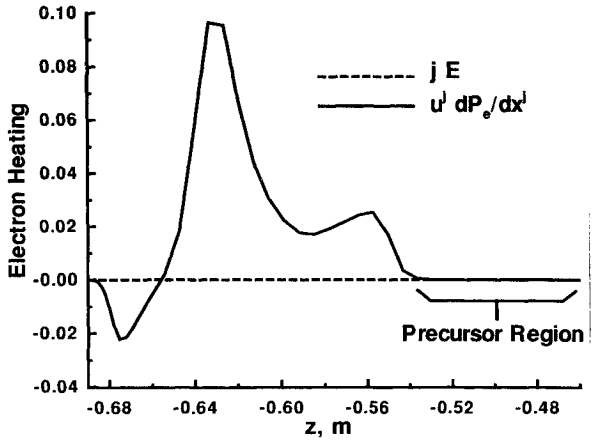

Fig. 8 Comparison of the original term accounting for electron heating with the additional ohmic heating term across the shock layer on the body flank ($x = 1.5$ m).

surface; these boundary conditions require B to be a constant 0.3 G at these two boundaries also. Zeroth-order extrapolation fixes the value of B across the shock layer at the downstream exit boundary on the body's flank.

Plasma Electrical Conductivity

An additional transport coefficient, the plasma electrical conductivity, is required to solve the magnetic induction equation. For simple plasmas at energies less than 50 eV, Braginskii[14] suggests a Spitzer[15] formulation:

$$\sigma = 0.0153 T_e^{1.5}/\lambda \tag{16}$$

where

$$\lambda = \ell n \left[\frac{1.89506 \times 10^{16}\ T_e^{3.45}}{n_e^{1.15}} \right] \tag{17}$$

Although the high energy flow of air about an aerobrake is not a simple plasma, this relation is used in the present study (as it was used by Palmer[5]).

Test Case and Computational Grid

A primary test case characteristic of Earth re-entry upon return from Mars is examined. This case is selected because of its high degree of ionization (as high as 25%) and significant thermal nonequilibrium effects. Earth re-entry of aerobrakes returning from geosynchronous orbit or the Moon typically involve maximum ionization of less than 5%.

The axisymmetric geometry examined is a 60-deg sphere cone with nose radius of 1.1 m traveling 12 km/s at 80 km altitude. The magnetic induction equation is solved on the same grid as the gasdynamic equations. Three different computational grids will be examined. For each of these grids, cell Reynolds number for the first cell adjacent to the body is one. Grid lines normal to the body are locally orthogonal to the body surface. Tangential grid lines are aligned with the shock. The first grid examined has 24 cells along the body and 64 cells normal to the body. This grid and the axisymmetric aerobrake geometry are shown in Fig. 1. Two high-resolution, 30×128, grids are also examined. For these grids, the grid adaptation routine SAGE[16] is used to cluster points around the high gradient shock. These two grids are described in the next section.

Results

Solving the magnetic induction equation, Eq. (12), requires n_e, T_e, and u^j from the flowfield solution. Initially, a LAURA flowfield solution, computed for the test case without the added plasmadynamic terms, is used to compute the magnetic field. The magnetic fields computed in this manner are referred to as "uncoupled" solutions. Grid resolution studies and term-by-term examination of the magnetic induction equation are performed on uncoupled solutions. A "coupled" solution is then computed by combining the solution of the magnetic field with the solution of the flowfield.

Temperature profiles across the shock layer on the body flank ($x = 1.5$ m) for the uncoupled LAURA flowfield solution are shown in Fig. 2. The shock is clearly shown by the steep rise in translational temperature. The postshock region where T and T_V differ indicates the significant thermal nonequilibrium effects present in this case. LAURA utilizes a two-temperature model; the T_e required for the solution of the magnetic field is T_V. Contours of the uncoupled magnetic field predicted for this flowfield are shown in Fig. 3. In the nose region, the magnetic field grows from its freestream boundary value of 0.3 G to a maximum value of 0.33, then decreases to 0.19 before rising back to the ambient value at the wall. The maximum strength of the field is 0.40 on the flank of the body. The magnetic field is not strong (although it is the gradients in the field that are important).

Resolution Study

Little experience exists in computing the magnetic field about aerobrakes. To establish confidence in the computed electromagnetic field, grid refinement, grid extent, and spatial accuracy of the differencing are examined. To examine grid resolution effects, a second uncoupled LAURA solution is computed for just the nose region of this vehicle on a SAGE-adapted 30×128 grid. In the neighborhood of the shock, grid cells on this high-resolution grid are a factor of 30 smaller than for the original 24×64 grid. The induced magnetic field computed on this grid is shown in Fig. 4. Increased grid resolution does not change the solution significantly.

The uncoupled magnetic induction equation is resolved for this case using fourth-order accurate spatial differencing on the high-resolution grid. The resulting magnetic field is shown in Fig. 5. Although the extrema of the field are changed due to higher order differencing (the minimum value computed for B is 0.16 for this solution), the solution is similar to that of Fig. 4.

LAURA is a shock-capturing scheme. The freestream grid boundary is usually placed at 125% of the shock standoff distance. Examining Figs. 3–5 reveals that the magnetic field is not constant in the region outside of the shock: the shock precursor region. The flowfield and electromagnetic field for the nose region of the test case are computed on another 30×128 grid that extends to 165% of the shock standoff distance. The resulting magnetic field is shown in Fig. 6. This increased-grid-extent solution has a slightly different structure than that of Fig. 4. The objective of the present study is to

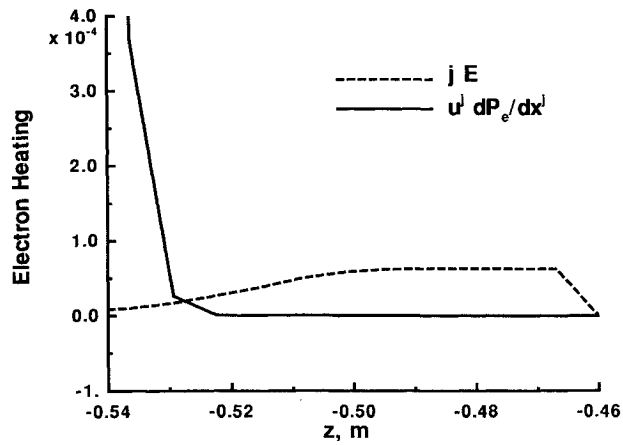

Fig. 9 Enlarged view of the precursor region for comparison of the original term accounting for electron heating with the additional ohmic heating term.

estimate the importance of plasmadynamic effects on aerobrake flows. Increased grid resolution, grid extent, and spatial accuracy of the differencing have an effect on the solution. To satisfy the qualitative objectives of this study, however, the original 24×64 grid of Fig. 1 (magnetic field in Fig. 3) is adequate.

Source of the Magnetic Field

Individual terms in the magnetic induction equation are examined next. The magnetic induction equation, Eq. (12), is composed of the standard MHD terms, a "Hall" term, and the thermoelectric term. When the Hall term is omitted, the electromagnetic solution is unchanged. For the remainder of the results presented in this study, this term is neglected. When the thermoelectric term is also omitted, the resulting magnetic field is shown in Fig. 7. This is the standard MHD solution. The thermoelectric term, as pointed out by Shebalin,[4] is an important term in creating gradients in the magnetic field. Comparison of Fig. 7 with Fig. 3 reveals that the thermoelectric term can act as both source and sink of field strength. This is a surprising observation since the thermoelectric term,

$$\frac{k}{e}\nabla T_e \times \nabla \ell n\, n_e \tag{18}$$

is the cross product of electron temperature gradient and the electron number density gradient that "should" be aligned for a blunt-body flow. In reality, the two gradients are not precisely aligned, especially deep in the shock layer where electron impact ionization releases an avalanche of free electrons. This misalignment results in a nonzero value for the term in Eq. (18) that induces electromagnetic fields and currents.

Coupled Two-Temperature Solution

The "uncoupled" magnetic fields computed earlier are not strong. It is, however, the gradient of the magnetic field that appears as the magnetic force term in the total momentum equation and the ohmic heating term in the vibrational-electron-electronic energy and total energy equations. The ohmic heating term in Eq. (7) is the important coupling term. Figure 8 compares this added ohmic heating term, $j\cdot E$, with the original term used to account for the work done on the electrons by the electric field. The plot is across the shock layer in the region of maximum ohmic heating ($x = 1.5$ m). The sum of these two terms is what now accounts for electron heating. On the scale of this plot, the new additional term is negligible across the entire shock layer. Figure 9 presents a closeup of this comparison in the shock precursor region. Both terms are near zero in this region. The ohmic heating, however, is not

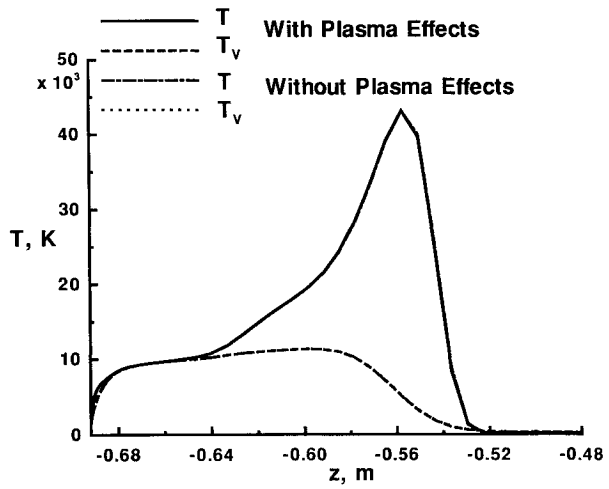

Fig. 10 Comparison of the temperature profiles across the shock layer on the body flank ($x = 1.5$ m) with and without plasmadynamic effects.

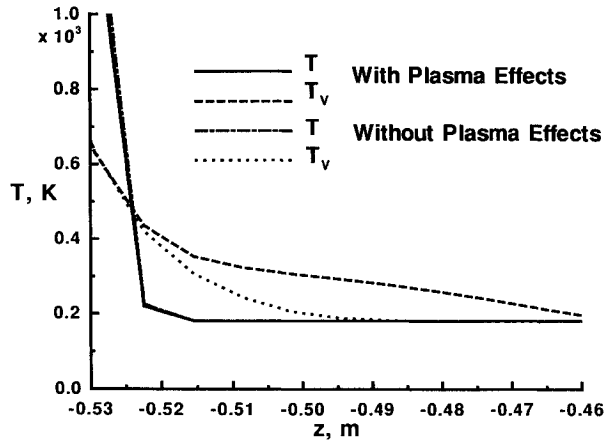

Fig. 11 Enlarged view of the precursor region for the comparison of temperature profiles across the shock layer on the body flank ($x = 1.5$ m) with and without plasmadynamic effects.

negligible in this region because the remainder of the terms in the vibrational-electronic-electron energy equation are also very small in this region. Figures 8 and 9 reveal that the only possible region where plasma effects might affect the flowfield is in the shock precursor region.

A coupled solution for the flowfield/electromagnetic field under the two-temperature assumption of LAURA is computed on the 24×64 grid to determine the impact of this effect. The inclusion of plasmadynamic effects has no noticeable impact on the predicted surface pressure and heating. The coupled magnetic field is unchanged from that of Fig. 3. The electron number densities are likewise unaffected. The only noticeable effect on the flowfield results from the nonzero ohmic heating shown in Fig. 9. The effect is a slight increase in T_V just ahead of the shock. Figure 10 is a comparison of the temperature profiles across the entire shock layer on the body flank ($x = 1.5$ m) for the solution without plasma effects and the coupled solution. Figure 11 presents a closeup of the precursor region. This is the effect of ohmic heating. The increase in temperature of only 100 K, however, does not result in any other impact on the flowfield.

Another coupled two-temperature solution is computed for re-entry conditions characteristic of return from the Moon. The representative axisymmetric geometry is a 70-deg sphere cone with base radius of 7 m. Freestream velocity is 9834 m/s at 75 km altitude. The maximum degree of ionization is only 5% for this case. Again, including plasmadynamic effects in the solution does not alter any of the flowfield variables except the temperature profiles in the shock precursor region. Though not shown, the effect is similar to that shown in Fig. 11. It is interesting to note that this small effect does not appear to depend on the degree of ionization in the flowfield.

Three-Temperature Considerations

Justification of the two-temperature assumption based on Hansen's estimate of the electron-electronic to vibrational energy relaxation rate was presented earlier. If Hansen's estimate is not correct, and the relaxation of electron-electronic energy into the vibrational and other modes is not that fast, what macroscopic effect could large electron temperatures in the shock precursor region produce? Highly energetic electrons can cause electron impact ionization of the molecules of the gas, resulting in an increase in electron number density, or the energetic electrons might be captured in free-bound transitions, giving up their energy as radiation. If all of the ohmic heating energy cited earlier is immediately used to ionize N_2 molecules, however, only 0.0005% ionization of the freestream would occur. (The first ionization energy of N_2 is 15.51 eV.) Such small degree of ionization would have no noticeable effect on the flowfield. Furthermore, if all of the ohmic heating is converted to radiation and transmitted to the body

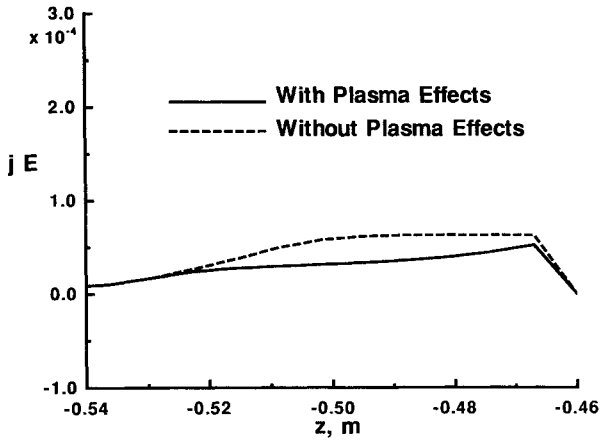

Fig. 12 Effect of coupling plasmadynamic effects on ohmic heating in the shock precursor region of the body flank ($x = 1.5$ m) for the two-temperature solution.

surface, the effect is still negligible. The amount of energy being added to the flow due to ohmic heating in this region is approximately 0.004 J/m^3. Compared with the freestream energy of 2.7 J/m^3, this is a small amount of energy addition. (The vibrational-electron-electronic energy of the freestream is 0.08 J/m^3, which is why a small effect on T_V occurs in Fig. 11 due to the ohmic heating of 0.004 J/m^3.)

There remains one possibility to consider. The induced magnetic field is a function of T_e. The change in T_e in the precursor region that a three-temperature model would allow might alter the magnetic induction solution in such a way as to increase the ohmic heating. If this were true, the situation would constitute an instability where the ohmic heating might grow until it is no longer a negligible term. Restated, the question is, what is the "feedback" effect of increased electron temperature on the ohmic heating term? The answer can be approximated by examining the trend observed in the two-temperature solution. Figure 12 compares the ohmic heating of the uncoupled solution with the coupled solution in the precursor region. The coupling of the plasmadynamic effects with the flowfield acts to increase T_V in the two-temperature solution as shown in Fig. 11 as it would increase T_e in a three-temperature solution. As Fig. 12 shows, this *decreases* the ohmic heating. The previously misaligned gradients of electron temperature and number density in the thermoelectric term are being realigned by the coupling effects. There is no evidence to suggest that the three-temperature model would exhibit different behavior. The feedback effect of coupling plasma effects to a three temperature model may also decrease the ohmic heating.

Based on the above arguments of electron-vibrational relaxation time, magnitude of the ohmic heating, and feedback effect on the ohmic heating, a three temperature model should not produce any significantly different conclusions then those drawn from the two-temperature results.

Conclusions

Including plasmadynamic effects in the governing equations of hypersonic flow requires the addition of a magnetic force term to the momentum equations and an ohmic heating term to the electron and total energy equations. Closure of the resulting equation set requires solution of the magnetic induction equation as an additional field equation and the specification of an additional transport coefficient: the plasma electrical conductivity.

The magnetic field about a 1.1-m nose-radius aerobrake entering Earth's atmosphere at 80 km altitude and traveling 12 km/s is computed. Results from the Spitzer relation for the plasma electrical conductivity indicate that the induced magnetic field is weak with values between 0.1–0.5 G for freestream values of 0.3 G.

Grid resolution and grid extent studies suggest that the computational grid used for the flowfield provides sufficient resolution for computing the magnetic field. In addition, second-order accurate spatial differencing of the magnetic induction equation is adequate.

The thermoelectric term in the magnetic induction equation is an important source of the weak magnetic fields for aerobrake flows. This is an unexpected observation since this term is the cross product of two gradients that were assumed to be aligned. The Hall term in the magnetic induction equation does not contribute to the magnetic field strength since the field strengths remain small.

The induced magnetic field has associated currents that cause an increase in the energy of the free electrons due to ohmic heating. This energy addition is small, 0.005 W/cm^3, but in the preshock region must be distributed over a very small number of electrons. If, as is assumed in a two-temperature approximation, the electrons instantly equilibrate with the bound electrons and the vibrational states of the molecules, the energy added due to ohmic heating results in a small increase in the vibrational temperature in the shock precursor region. This effect is negligible and no other noticeable effect on the flowfield, surface pressure, or heating is seen. These conclusions agree with those of Palmer.[5] In addition, a two-temperature solution for a lunar return aerobraking case at 9834 m/s and 75 km altitude did not produce any important effects on the flowfield. An estimate of the electronic-vibrational relaxation time indicates that the two-temperature assumption employed in this study is valid for air. By examining the magnitude of the ohmic heating and observing a decrease in this heating when coupling terms are included in the two-temperature solution, a three-temperature solution should not produce significantly different conclusions.

The conclusions of this work are restricted to Earth-entry aerobraking. Entering the atmospheres of the other planets, like the hydrogen-rich atmosphere of Jupiter, may involve significant plasmadynamic effects.

Acknowledgments

The authors would like to thank Peter Gnoffo and Frederick Hansen for many helpful discussions during the course of this work. William Kleb was also helpful in implementing the SAGE grid-adaptation routine.

References

[1]Mitcheltree, R. A., and Gnoffo, P. A., "Thermochemical Nonequilibrium Issues for Earth Reentry of Mars Mission Vehicles," *Journal of Spacecraft and Rockets,* Vol. 28, No. 5, 1991, pp. 552–558; see also AIAA Paper 90-1698, June 1990.

[2]Mitcheltree, R. A., "Parametric Study of Dissociation and Ionization Models at 12 Kilometers/Second," *Journal of Spacecraft and Rockets,* Vol. 28, No. 6, 1991, pp. 619–627; see also AIAA Paper 91-1368, June 1991.

[3]Tauber, M. E., Palmer, G., and Yang, L., "Earth Atmospheric Entry Studies for Manned Mars Mission," AIAA Paper 90-1699, June 1990.

[4]Shebalin, J. V., "Aerobrake Plasmadynamics: Macroscopic Effects," *Journal of Spacecraft and Rockets,* Vol. 28, No. 4, 1991, pp. 394–400; see also AIAA Paper 90-1559, June 1990.

[5]Palmer, G., "The Effects of Self-Generated and Applied Magnetic Fields on the Computation of Flow over a Mars Return Aerobrake," AIAA Paper 91-1462, June 1991.

[6]Lee, J. H., "Basic Governing Equations for the Flight Regimes of Aeroassisted Orbital Transfer Vehicles," *Thermal Design of Aeroassisted Orbital Transfer Vehicles,* edited by H. F. Nelson, Vol. 96, Progress in Astronautics and Aeronautics, AIAA, New York, 1985, pp. 3–53.

[7]Hirschfelder, J. O., Curtiss, C. F., and Bird, R. B., *Molecular Theory of Gases and Liquids,* Wiley, New York, 1954.

[8]Gnoffo, P. A., Gupta, R. N., and Shinn, J. L., "Conservation Equations and Physical Models for Hypersonic Air Flows in Thermal and Chemical Nonequilibrium," NASA TP-2867, Feb. 1989.

[9]Park, C., "Assessment of Two-Temperature Kinetic Model for Ionizing Air," AIAA Paper 87-1574, June 1987.

[10]Hansen, F. J., private communication, Univ. of Oregon, Eugene, OR, Aug. 1991.

[11]Park, C., Howe, J. T., Jaffe, R. L., and Candler, G. V., "Chemical-Kinetic Problems of Future NASA Missions," AIAA Paper 91-0464, Jan. 1991.

[12]Gupta, R. N., Yos, J. M., Thompson, R. A., and Lee, K. P., "A Review of Reaction Rates and Thermodynamic and Transport Properties for an 11-Species Air Model for Chemical and Thermal Nonequilibrium Calculations to 30000 K," NASA RP-1232, Aug. 1990.

[13]Gnoffo, P. A., "An Upwind-Biased, Point-Implicit Relaxation Algorithm for Viscous, Compressible Perfect-Gas Flows," NASA TP-2953, Feb. 1990.

[14]Braginskii, S. I., "Transport Processes in a Plasma," *Reviews of Plasma Physics,* Vol. 1, Consultants Bureau, New York, 1965, pp. 205–292.

[15]Spitzer, L. J., *Physics of Fully Ionized Gasses,* Wiley, New York, 1962.

[16]Davies, C., and Venkatapathy, E., "Application of a Solution Adaptive Grid Scheme, SAGE, to Complex Three-Dimensional Flows," AIAA Paper 91-1594, June 1991.

Ernest V. Zoby
Associate Editor